Computational Materials Science 95 (2014) 563–567

Contents lists available at ScienceDirect

Computational Materials Science

journal homepage: www.elsevier.com/locate/commatsci

Doping-dependent thermoelectric properties of $BiSb_3Te_6$ from first-principle calculations

Songke Feng, Shuangming Li *, Xin Li, Hengzhi Fu

State Key Laboratory of Solidification Processing, Northwestern Polytechnical University, Xi'an 710072, PR China

ARTICLE INFO

Article history:
Received 28 June 2014
Received in revised form 13 August 2014
Accepted 14 August 2014
Available online 15 September 2014

Keywords:
First-principle calculations
$BiSb_3Te_6$ material
Electronic structure
Thermoelectric properties
Carrier concentration

ABSTRACT

The influence of electronic structure and doping level on the thermoelectric transport properties of $BiSb_3Te_6$ compound was investigated using first-principle calculations and Boltzmann transport theory. The calculation results indicate that $BiSb_3Te_6$ is a narrow gap semiconductor with an indirect band gap of 0.113 eV. The calculated band structures of the compound present nonparabolic curves with multi-valley band property. The density of states is enhanced below a few tenths of Fermi energy and the bands are flatted with heavy effective mass. The calculated thermoelectric coefficients of $BiSb_3Te_6$ are anisotropic and mainly dependent on the doping concentrations. The dopant dependences of *ZT* values are given with the optimal carrier concentrations $\sim 10^{19}$ cm^{-3}. This theoretical investigation gives a valuable insight into the relationship between the electronic structure and thermoelectric transport properties of $BiSb_3Te_6$ material, and provides a quantificational doping level to improve the thermoelectric performance.

1. Introduction

Thermoelectric material (TM) provides a useful solid-state conversion technology for refrigeration and power generation [1–4]. The conversion efficiency of TM devices is limited by a dimensionless figure of merit $ZT = S^2\sigma T/k$, where S is the Seebeck coefficient, T is the absolute temperature, σ is the electrical conductivity, and k is the thermal conductivity which generally includes the contributions of phonons k_l and electrons k_e. High performance TM requires a large power factor ($S^2\sigma$) and a low thermal conductivity. Finding a superior *ZT* material is full of challenges due to the conflicting thermoelectric parameters (S, σ, and k_e). These thermoelectric coefficients are highly dependent on interrelated material carrier concentration and need to be optimized to maximize *ZT* [5,6].

At room temperature (up to 500 K), $BiSb_3Te_6$ is one of the best performances TMs with peak *ZT* values of 0.96–1.4 [7,8]. To further improve the thermoelectric property of $BiSb_3Te_6$ compound, one way is to reduce the thermal conductivity of the compound. It was reported that a minimal k_l can reach 0.22 $W\,m^{-1}\,k^{-1}$ [9]. However, the obtained *ZT* was less than 1.5 due to its lower power factor (*PF*) of inappropriate carrier concentration. Another method is developed to optimize the power factor by adjusting the carrier concentration. A maximum *PF* of 7.21 $\mu W\,cm^{-1}\,k^{-2}$ has been obtained in $BiSb_3Te_6$ material [10]. In addition, a small quantity of Mn [11], Cu [12] and Ag [13] elements were introduced into $BiSb_3Te_6$ compound to modulate the carrier concentration. Although these reports suggested that the proper doping concentration should be in the scope of 10^{19}–10^{21} cm^{-3}, they have not provided the carrier concentration of the higher power factor required. The quantitative doping range of higher *ZT* is still lacking, to the best of authors' knowledgement.

In view of this, the purpose of this study is to provide predictions of the dependence of the thermoelectric coefficients on carrier concentration with the Boltzmann transport theory using the full electronic structure, giving reasonable doping levels to optimize the thermoelectric properties of $BiSb_3Te_6$ material.

2. Calculation methods and theory

2.1. Calculated methods

The crystal structure of bulk $BiSb_3Te_6$ was constructed substituting one Bi atom for Sb atom in a $1 \times 1 \times 2$ supercell of the nominal formula Sb_4Te_6, as shown in Fig. 1. To confirm the stability of the crystal, a negative formation heat of −1.42 eV was obtained by calculating $E_{(BiSb3Te6)} + E_{(Sb)} - 2E_{(Sb2Te3)} - E_{(Bi)}$. The optimized lattice constants are $a = 4.33$ Å and $c = 30.40$ Å, which are very close to the experimental data of $a = 4.28$ Å and $c = 30.49$ Å [14]. These results suggest that the $BiSb_3Te_6$ crystal is a stable compound and can be synthesized experimentally.

* Corresponding author. Tel./fax: +86 029 88493264.
E-mail address: lsm@nwpu.edu.cn (S. Li).

http://dx.doi.org/10.1016/j.commatsci.2014.08.028
0927-0256/

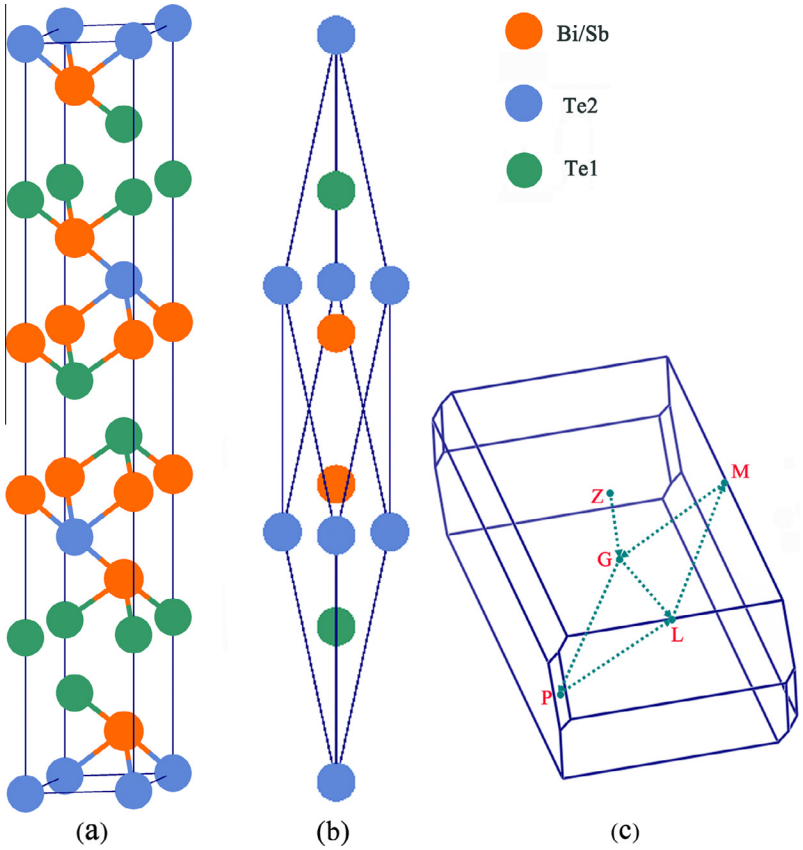

Fig. 1. The layered (Bi, Sb)$_4$Te$_6$ crystal structure (a) was constructed from the Sb$_2$Te$_3$ unit cell, (b) by replacing Sb with Bi atom. The building Brillouin zone (c) and the high-symmetry points were based on the $1 \times 1 \times 2$ supercell.

Based on the density functional theory, our calculations were performed using full-potential linearized augmented plane-wave (LAPW) [15] method as implemented in WIEN2K code [16]. The generalized gradient approximation with the Perdew–Burke–Ernzerho (PBE) [17] and Engel–Vosko (EV) [18] was applied to evaluate exchange–correlation energy. The PBE–GGA was used to calculate the structural properties. The band-structure properties were computed using the EV–GGA, which was a very accurate function in determining the electronic structure of thermoelectric materials [19–21]. LAPW spheres of radii 2.5 Bohr were employed for both Bi, Sb and Te atoms, with well-converged basis sets determined by $\min(R_{MT})\max(k_n) = 7.0$, where R_{MT} is the minimum LAPW radius and k_n is the plane-wave cutoff. Because Bi, Sb and Te are heavy elements, the relativistic $p_{1/2}$ local orbital [15] is introduced in the spin–orbit (SO) calculations.

An $8 \times 8 \times 6$ Monkhorst–pack k-point sampling was applied in the irreducible Brillouin zone (BZ). The crystal structure was relaxed by the BFGS method [22] for both lattice parameters and atomic internal coordinates until the stress along each lattice direction was less than 0.02 kbar, and the total energy less than 0.0001 eV. The electronic structure was calculated in the optimized crystal structure with $32 \times 32 \times 24$ denser grids. Thermoelectric transport coefficients were derived from the electronic structure with the Boltzmann transport theory.

2.2. Boltzmann transport theory

The thermoelectric parameters were calculated by resolving the Boltzmann transport equation with the constant relaxation time approximation (CRTA) [20]. The transport coefficients of electrical conductivity σ, Seebeck coefficient S, and electronic thermal conductivity k_e are given by the following equations [19]:

$$\sigma(T,\mu) = X^{(0)} \tag{1}$$

$$S(T,\mu) = \frac{1}{eT}\left(2X^{(0)}\right)^{-1}X^{(1)} \tag{2}$$

$$k_e(T,\mu) = \frac{1}{e^2T}X^{(2)} \tag{3}$$

$$X^{(n)} = \frac{1}{\Omega}\int \sigma_{\alpha\beta}(\varepsilon)(\varepsilon-\mu)^n\left(-\frac{\partial f_\mu(T,\varepsilon)}{\partial\varepsilon}\right)d\varepsilon \tag{4}$$

where the symbol e is the electrical charge, T is the Kelvin temperature, Ω is the reciprocal space volume, ε is the energy to the corresponding k point, μ is the chemical potential, and f is the Fermi distribution function. The conductivity tensors $\sigma_{\alpha\beta}$ [23] is written as:

$$\sigma_{\alpha\beta}(\varepsilon) = \frac{e^2\tau}{N}\sum_{i,k} v_a(k)v_\beta(k)\frac{\delta(\varepsilon-\varepsilon_k)}{d\varepsilon} \tag{5}$$

where τ is the relaxation time, $v_a(k)$ is the electrical group velocity, and N is normalization depending on the number of k points sampled in the BZ. For resolving these equations, we adopt τ as a constant without variation on the scale of a few kT in the inelastic scattering regime. This is usually applied to degenerately doped semiconductors and metals, obtaining many reasonable results between the calculations and experiments [24–28].

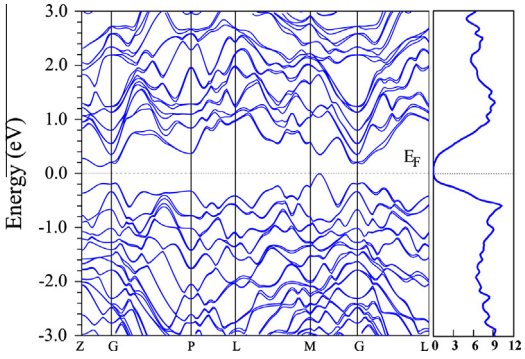

Fig. 2. Electronic DOS and band structure of the $BiSb_3Te_6$ crystal calculated using the EV–GGA along the high-symmetry points in the first Brillouin zone.

3. Results and discussions

3.1. The electronic structure

The calculated density of states and band structures of the $BiSb_3Te_6$ crystal along the high symmetry lines are plotted in Fig. 2. It indicates that the crystal is a narrow-gap semiconductor with an indirect band gap E_g of 0.113 eV. This result agrees well with the experimental data of 0.112 eV [29], but is lower than the value of 0.19 eV [30,31]. The Fermi level approaches the valence bands, with the implication that the crystal is a *p*-type semiconductor with the hole-transport property. From the band structures of Fig. 2, the conduction-band maximum is along *G–Z* direction. Along this direction, a relative flat band is observed, leading to the formation of heavy effective mass and lower carrier mobility. Unlike the conduction-band structures, the valence-band maximum is along *G–M* direction and the Fermi energy is close to the peak point of the valence band. With dropping the energy, about 0.2 eV, into the band edge of *G* point, the valence bands become heavier. The heavy bands are attributed to the strong effect of spin–orbit interactions in the $BiSb_3Te_6$ crystal, which is very similar to the Bi_2Te_3 compound [32,33].

In addition, the density of states (DOS) rapidly increases with lowering a few tenths of the Fermi energy into the valence bands. This rapid change of DOS is beneficial to improve the thermoelectric power of the TMs [34,35]. Meanwhile, the $BiSb_3Te_6$ crystal presents multivalley band structures and these bands are highly nonparabolic, which are contributable to the enhancement of thermoelectric performance at elevated temperature and doping level [7,36].

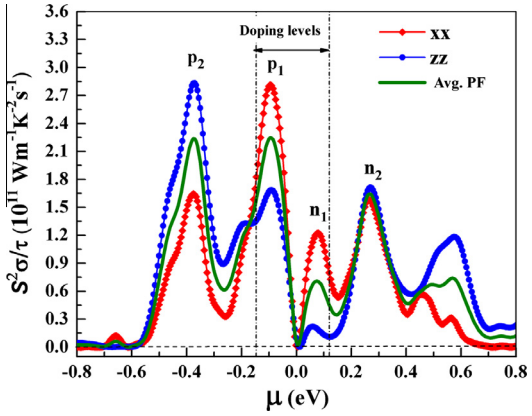

Fig. 4. Calculated power factor (*PF*) as a function of chemical potentials for both *n*-type and *p*-type doping at room temperature. The reasonable doping levels are in a region between the half values of the maximum *PF* at p_1 and n_1 points.

3.2. The transport coefficients

Fig. 3a shows the calculated room-temperature Seebeck coefficients in-layer (along the cleavage plane) S_{xx}, and cross-layer (*zz*) S_{zz} with both *n*-type and *p*-type doping. The Seebeck coefficients of *p*-type doped crystal increase rapidly than that of *n*-type doped crystal, reaching the maximum values of 253 μV K^{-1} and −185 μV K^{-1}. They are very close to the experimental results of 256 μV K^{-1} [6] and 255 μV K^{-1} [13], but larger than that of −149 μV K^{-1} [6]. According to Mott theory [35], the improvement of Seebeck coefficients closely links with the variation of the DOS near Fermi energy. Therefore, higher Seebeck coefficients in this calculation originate from the rapidly changing DOS, as plotted in Fig. 2. This enhancement of Seebeck coefficients has also been experimentally proved in the PbTe,Tl compound [37].

As indicated in Fig. 3a, we also observe the $BiSb_3Te_6$ crystal displaying isotropic Seebeck effect. The extreme points of Seebeck coefficient are within the scope of the energy gap; it implies that the Seebeck coefficient can be improved by adjusting the Fermi energy. In contrast to the Seebeck coefficient, the electrical conductivity is anisotropic for both *p*-type and *n*-type materials. The ratio of σ_{xx}/σ_{zz} reaches ~4.5 for *n*-type doping, and ~1.5 for *p*-type doping, as shown in Fig. 3b. Such a strong anisotropic electrical conductivity is very similar to the layered Bi_2Te_3 crystal [38].

Fig. 4 is the comprehensive transport parameter *PF* with the extreme points (p_1, p_2, n_1, n_2) located at different chemical potential for both *p*- and *n*-type materials. The chemical potentials with

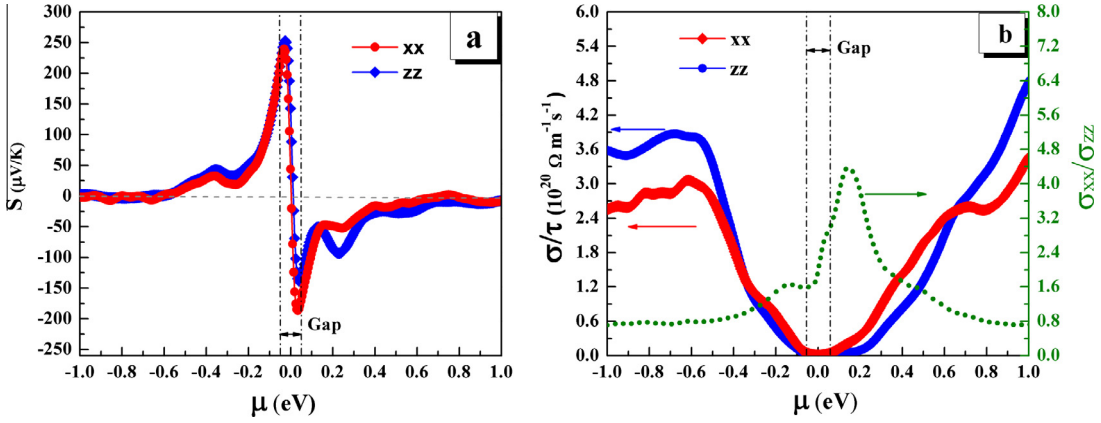

Fig. 3. Calculated room-temperature transport coefficients of Seebeck coefficient (a) and electrical conductivity and (b) are plotted as a function of the chemical potential for both *n*-type and *p*-type doping. Symbols of *xx* and *zz* are parallel and perpendicular to the cleavage plane, respectively.

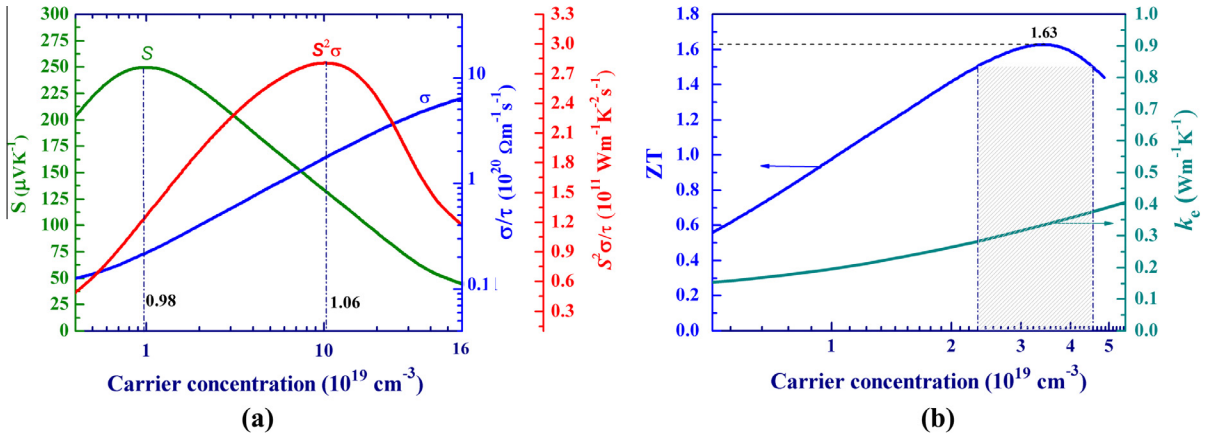

Fig. 5. The dopant dependence of the room-temperature thermoelectric coefficients: S, σ and PF (a), ZT and electronic k_e (b).

respect to p_1 and n_1 points are −0.101 eV and 0.074 eV, respectively. These two peak points are within the feasible doping levels because they approach the edge of the conduction band (n-type) and valence band (p-type). However, p_2 and n_2 points are located at heavy doping concentrations ($\sim 10^{21}$ cm^{-3}), in which a large k_e is introduced into TMs and thus lowers the ZT values. In this calculation, the available doping levels therefore are in a region between the half values of the maximum PF at p_1 and n_1 points. They can be limited to a range between −0.15 eV(p-type) and +0.12 eV(n-type), corresponding to the carrier concentration from $+2.8 \times 10^{20}$ cm^{-3} to -8.5×10^{19} cm^{-3}.

Additionally, the average power factors using the data calculated from the xx- and zz-planes are drawn with the solid line in Fig. 4. The optimized PF at p_1 point reaches 2.25×10^{11} W m^{-1} K^{-2} s^{-1}, about 7.2×10^{-3} W m^{-1} K^{-2} if τ is set at 3.2×10^{-14} s, in good agreement with the experiment data of 7.24 W m^{-1} K^{-2} by Zhao et al. [10]. Introducing the experimental thermal conductivity of 1.6 W m^{-1} K^{-1} [39,40], at 300 K, the average dimensionless figure of merit ZT could reach 1.35, closes to 1.2 as reported by Poudel et al. [41]. At this optimal doping concentration, the ZT value could be further improved in the even lower thermal-conductivity nanoscale compound.

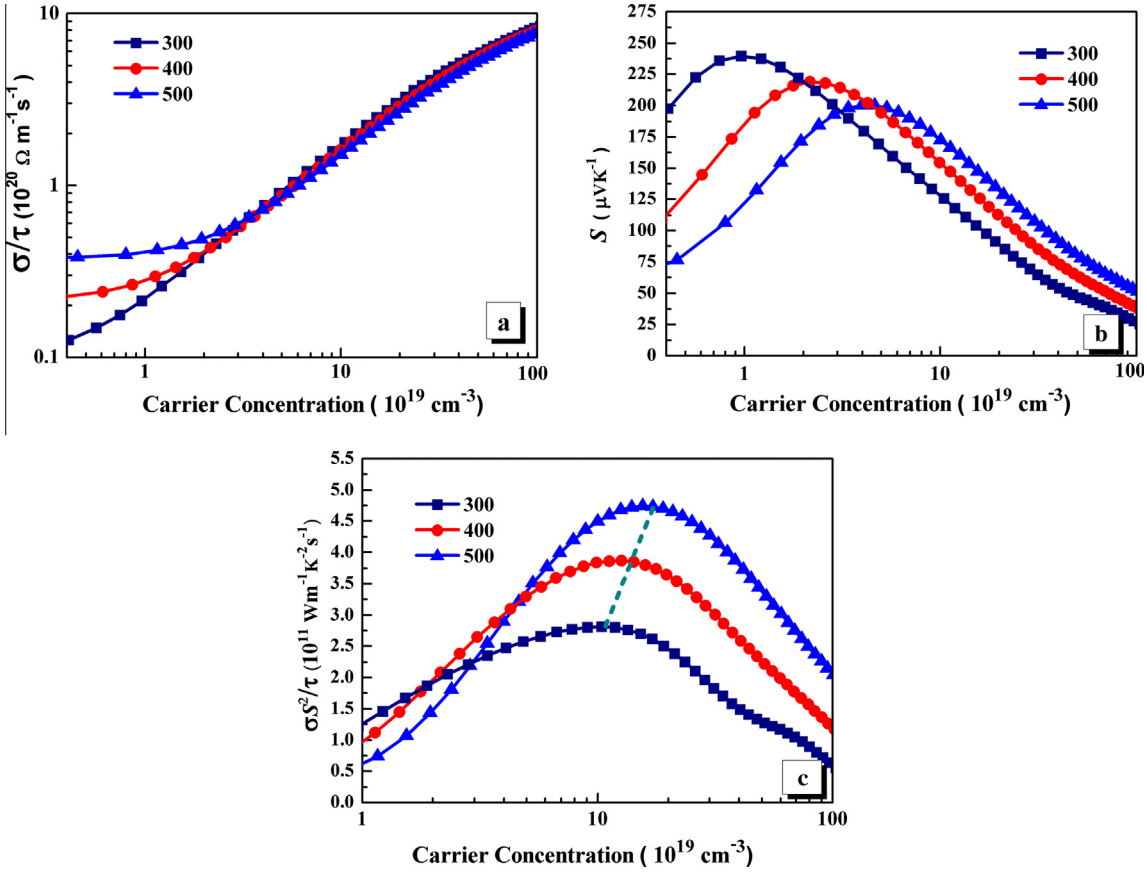

Fig. 6. Calculated in-plane electrical conductivity (a), Seebeck coefficient (b) and power factor (c) as a function of carrier concentration in p-type doped $BiSb_3Te_6$ materials at 300–500 K.

3.3. The thermoelectric properties at different doping levels

Fig. 5a displays the carrier concentration dependence of thermoelectric parameters for the *p*-type doped compound at room temperature. It implies that with increasing the doping concentration, the electrical conductivity continuously increases and the Seebeck coefficient first rises and then reduces. As the doping concentration is over 9.8×10^{18} cm^{-3}, the Seebeck coefficient and electrical conductivity change in opposite direction with increasing the doping levels, resulting that the optimum power factor does not match with the optimum Seebeck coefficients. Here, the maximum *PF* can reach 2.78×10^{11} W m^{-1} K^{-2} s^{-1} at $n = 1.06 \times 10^{20}$ cm^{-3}.

High carrier concentration $BiSb_3Te_6$ semiconductors have large power factor. However, high carrier concentration also results in large electronic thermal conductivity k_e. As shown in Fig. 5b, the electronic thermal conductivity k_e attains 0.4 W m^{-1} K^{-1} at the doping level of 5.5×10^{19} cm^{-3}, approaching the same order of magnitude of the lattice thermal conductivity 0.7 W m^{-1} K^{-1} [30]. By combining the available experimental thermal conductivity [42] with our calculated *PF*, the largest *ZT* value is up to 1.64 at the carrier concentration of 3.5×10^{19} cm^{-3}. This predicted figure of merit (*ZT*) is in good agreement with the experimental result of 1.56 reported by Jiang et al. [8]. If the *ZT* value need exceed 1.5, the optimized carrier concentration should be within the doping range 2.32×10^{19}–4.55×10^{19} cm^{-3}. Additionally, assuming that the lattice thermal conductivity k_l may suppress small enough ($\sim$0.8 W m^{-1} K^{-1}) at room temperature, the *ZT* value of the *p*-type doped $BiSb_3Te_6$ compound can break through 3, larger than the currently reported $ZT = 2.6$ in SnSe crystals [43].

In general, the doped $BiSb_3Te_6$ materials are primarily used for thermoelectric generator at 300–500 K [44]. Fig. 6 illustrates the effect of doping levels on the thermoelectric transport properties of the doped $BiSb_3Te_6$ materials along the cleavage plane at elevated temperatures. It can be observed that the temperatures have an influence on the electrical conductivity and Seebeck coefficient at the doping level below 1.5×10^{19} cm^{-3}. After that, as shown in Fig. 6a, the electrical conductivity is independent of the temperature and grows up linearly with increasing the carrier concentration.

In heavy doping region (>10^{20} cm^{-3}), as shown in Fig. 6b, the increase in temperature results in a high Seebeck coefficient. The accelerated rate of Seebeck coefficient with temperature can reach 0.2 μV K^{-2}. Since the *PF* ($S^2\sigma$) is more sensitive to the Seebeck coefficient than electrical conductivity, as displayed in the dot lines of Fig. 6c, the extreme point of the *PF* lifts to the high doping level with increasing the temperature. The optimized *PF* values are therefore improved with the elevating temperature and carrier concentration. This variation of the optimal *PF* yields functionally graded thermoelectric materials that are available for improving the coefficient of performance of the thermoelectric power generator.

4. Conclusions

First-principle calculations were used to investigate the electronic structure and thermoelectric properties for the $BiSb_3Te_6$ alloy. Similar to Bi_2Te_3, $BiSb_3Te_6$ is a narrow-gap semiconductor with an indirect band gap of 0.113 eV, about 0.05 smaller than that of Bi_2Te_3. The band structures present multivalley characteristics. The Fermi energy is close to the valence-band maximum and with lowering energy $\sim$0.2 eV; the density of states for the crystal improves greatly and the valence bands become flat. Calculated thermoelectric coefficients of the $BiSb_3Te_6$ material perform anisotropic properties. Along the cleavage plane, maximum Seebeck coefficients of 253 μV K^{-1} and −185 μV K^{-1} are obtained for both *p*-type and *n*-type materials, respectively. The electrical conductivity of the material in-layer is $\sim$4.5 times larger than that of cross-layer for the *n*-type doping, and $\sim$1.5 times for *p*-type doping. To acquire higher performance of doping $BiSb_3Te_6$ materials, the optimized carrier concentration should be within the range 2.32×10^{19} to 4.55×10^{19} cm^{-3}.

Acknowledgments

This work is supported by the National Natural Science Foundation of China (Nos. 50971101 and 51074127). The authors would also like to acknowledge the support received from the Center for High Performance Computing of Northwestern Polytechnical University, China.

References

[1] T.M. Tritt, M. Subramanian, MRS Bull. 31 (2006) 188–198.
[2] A. Shakouri, Annu. Rev. Mater. Res. 41 (2011) 399–431.
[3] Y. Pei, X. Shi, A. LaLonde, H. Wang, L. Chen, G.J. Snyder, Nature 473 (2011) 66–69.
[4] H. Lu, P.G. Burke, A.C. Gossard, G. Zeng, A.T. Ramu, J.H. Bahk, J.E. Bowers, Adv. Mater. 23 (2011) 2377–2383.
[5] G.J. Snyder, E.S. Toberer, Nat. Mater. 7 (2008) 105–114.
[6] Y. Zhao, J. Dyck, B. Hernandez, C. Burda, J. Am. Chem. Soc. 132 (2010) 4982–4983.
[7] H. Scherrer, S. Scherrer, Thermoelectrics Handbook: Macro to Nano, CRC Press Taylor & Francis Group, Boca Raton, 2006.
[8] Q. Jiang, H. Yan, J. Khaliq, H. Ning, S. Grasso, K. Simpson, M.J. Reece, J. Mater. Chem. A 2 (2014) 5785–5790.
[9] R. Venkatasubramanian, Phys. Rev. B 61 (2000) 3091–3097.
[10] Y. Zhao, J.S. Dyck, B.M. Hernandez, C. Burda, J. Am. Chem. Soc. 132 (2010) 4982–4983.
[11] T. Plechacek, P. Svanda, C. Draar, L. Benes, A. Krejá, P. Lostk, Radiat. Eff. Defects Solids 153 (2001) 343–358.
[12] J.L. Cui, H.F. Xue, W.J. Xiu, W. Yang, X.B. Xu, Scr. Mater. 55 (2006) 371–374.
[13] J.K. Lee, S.D. Park, B.S. Kim, M.W. Oh, S.H. Cho, B.K. Min, H.W. Lee, M.H. Kim, Mater. Lett. 6 (2010) 201–207.
[14] L.D. Ivanova, L.I. Petrova, Y.V. Granatkina, V.G. Leontyev, A.S. Ivanov, S.A. Varlamov, Y.P. Prilepo, A.M. Sychev, A.G. Chuiko, I.V. Bashkov, Inorg. Mater. 49 (2013) 120–126.
[15] L. Nordstrom, D.J. Singh, Planewaves, Pseudopotentials, and the LAPW Method, Springer, 2006.
[16] K. Schwarz, P. Blaha, Comput. Mater. Sci. 28 (2003) 259–273.
[17] J.P. Perdew, K. Burke, M. Ernzerhof, Phys. Rev. Lett. 77 (1996) 3865–3868.
[18] E. Engel, S.H. Vosko, Phys. Rev. B 47 (1993) 13164–13174.
[19] T.J. Scheidemantel, C. Ambrosch-Draxl, T. Thonhauser, J.V. Badding, J.O. Sofo, Phys. Rev. B 68 (2003) 125210.
[20] G.K.H. Madsen, D.J. Singh, Comput. Phys. Commun. 175 (2006) 67–71.
[21] D.J. Singh, Phys. Rev. B 81 (2010) 195217.
[22] D. Liu, J. Nocedal, Math. Program. 45 (1989) 503–528.
[23] L. Zhang, D.J. Singh, Phys. Rev. B 81 (2010) 245119.
[24] G.K. Madsen, D.J. Singh, Comput. Phys. Commun. 175 (2006) 67–71.
[25] A.F. May, D.J. Singh, G.J. Snyder, Phys. Rev. B 79 (2009) 153101.
[26] L. Lykke, B.B. Iversen, G.K.H. Madsen, Phys. Rev. B 73 (2006) 195121.
[27] G. Zhang, B. Li, Nanoscale 2 (2010) 1058–1068.
[28] S. Chen, K. Cai, C. Wang, Comput. Mater. Sci. 83 (2014) 12–15.
[29] M.K. Zhitinskaya, S.A. Nemov, L.D. Ivanova, Phys. Solid State 44 (2002) 42–47.
[30] D. Rowe, CRC Handbook of Thermoelectrics, CRC Press, Boca Raton, FL, 1995.
[31] M. Stordeur, H.T. Langhammer, H. Sobotta, V. Riede, Phys. Status Solidi (B) 104 (1981) 513–522.
[32] G. Wang, T. Cagin, Phys. Rev. B 76 (2007) 075201.
[33] S. Youn, A. Freeman, Phys. Rev. B 63 (2001) 85112.
[34] Y. Pei, H. Wang, G.J. Snyder, Adv. Mater. (2012) 1–11.
[35] J. Sootsman, D. Chung, M. Kanatzidis, Angew. Chem. Int. Ed. 48 (2009) 8616–8639.
[36] C. Herring, Bell Syst. Tech. J. 34 (1955) 237–290.
[37] J. Heremans, V. Jovovic, E. Toberer, A. Saramat, K. Kurosaki, A. Charoenphakdee, S. Yamanaka, G. Snyder, Science 321 (2008) 554.
[38] S.K. Mishra, S. Satpathy, O. Jepsen, J. Phys.: Condens. Matter 9 (1997) 461.
[39] Č. Drašar, A. Hovorková, P. Lošťák, H. Kong, C.-P. Li, C. Uher, J. Appl. Phys. 104 (2008) 023701.
[40] J. Cui, W. Xiu, H. Xue, J. Appl. Phys. 101 (2007) 123713.
[41] B. Poudel, Q. Hao, Y. Ma, Y. Lan, A. Minnich, B. Yu, X. Yan, D. Wang, A. Muto, D. Vashaee, X. Chen, J. Liu, M.S. Dresselhaus, G. Chen, Z. Ren, Science 320 (2008) 634–638.
[42] T. Caillat, M. Carle, P. Pierrat, H. Scherrer, S. Scherrer, J. Phys. Chem. Solids 53 (1992) 1121–1129.
[43] L.-D. Zhao, S.-H. Lo, Y. Zhang, H. Sun, G. Tan, C. Uher, C. Wolverton, V.P. Dravid, M.G. Kanatzidis, Nature 508 (2014) 373–377.
[44] M. Dresselhaus, G. Chen, Z. Ren, G. Dresselhaus, A. Henry, J. Fleurial, JOM – J. Min. Meta. Mater. Sci. 61 (2009) 86–90.